


# Cavity magnon polariton based precision magnetometry

Cite as: Appl. Phys. Lett. **117**, 144001 (2020); <https://doi.org/10.1063/5.0024369>

Submitted: 06 August 2020 . Accepted: 24 September 2020 . Published Online: 06 October 2020

N. Crescini , C. Braggio , G. Carugno, A. Ortolan , and G. Ruoso 



View Online



Export Citation



CrossMark



## Your Qubits. Measured.

Meet the next generation of quantum analyzers

- Readout for up to 64 qubits
- Operation at up to 8.5 GHz, mixer-calibration-free
- Signal optimization with minimal latency

Find out more



# Cavity magnon polariton based precision magnetometry

Cite as: Appl. Phys. Lett. **117**, 144001 (2020); doi: [10.1063/5.0024369](https://doi.org/10.1063/5.0024369)

Submitted: 6 August 2020 · Accepted: 24 September 2020 ·

Published Online: 6 October 2020



View Online



Export Citation



CrossMark

N. Crescini,<sup>1,2,a)</sup>  C. Braggio,<sup>2,3</sup>  G. Carugno,<sup>2,3</sup> A. Ortolan,<sup>1</sup>  and G. Ruoso<sup>1</sup> 

## AFFILIATIONS

<sup>1</sup>INFN-LNL, Viale dell'Università 2, 35020 Legnaro (PD), Italy

<sup>2</sup>Dipartimento di Fisica e Astronomia, Via Marzolo 8, 35131 Padova, Italy

<sup>3</sup>INFN-Sezione di Padova, Via Marzolo 8, 35131 Padova, Italy

Note: This paper is part of the Special Issue on Hybrid Quantum Devices.

<sup>a)</sup> Author to whom correspondence should be addressed: [nicolo.crescini@phd.unipd.it](mailto:nicolo.crescini@phd.unipd.it)

## ABSTRACT

A photon-magnon hybrid system can be realized by coupling the electron spin resonance of a magnetic material to a microwave cavity mode. The quasiparticles associated with the system dynamics are the cavity magnon polaritons, which arise from the mixing of strongly coupled magnons and photons. We illustrate how these particles can be used to probe the magnetization of a sample with a remarkable sensitivity, devising suitable spin-magnetometers, which ultimately can be used to directly assess oscillating magnetic fields. Specifically, the capability of cavity magnon polaritons of converting magnetic excitations to electromagnetic ones allows for translating to magnetism the quantum-limited sensitivity achieved by state-of-the-art microwave detectors. Here, we employ hybrid systems composed of microwave cavities and ferrimagnetic spheres to experimentally implement two types of novel spin-magnetometers.

Published under license by AIP Publishing. <https://doi.org/10.1063/5.0024369>

Among the most studied types of hybrid systems, an important role is played by photon-magnon hybrid systems (PMHSs).<sup>1,2</sup> These yielded remarkable results in the study of light-matter interaction,<sup>3</sup> and, in the last few decades, emerged as promising constituents for new quantum technologies as well.<sup>4–6</sup> PMHSs have different forms, as they are built with miscellaneous building blocks, but the underlying physics is similar. In a magnetic field  $B_0$ , a spin can change its quantum state from  $-1/2$  to a  $+1/2$  by absorbing a spin-1 boson, like a photon, and vice versa by the emitting one. In this sense, a quantum of spin excitation with energy  $\hbar\omega_m = \mu_B B_0$  can be effectively described as a quasiparticle, known as a magnon, which can turn into a photon of the same energy  $\hbar\omega_c$ .<sup>7</sup> This reciprocal conversion is quantified by the interaction strength  $g_{cm}$ , known as vacuum Rabi splitting, which is the rate at which magnons are converted into photons and vice versa. When  $g_{cm}$  is much larger than the damping rates of the magnon  $\gamma_m$  and of the photon  $\gamma_c$ , the system is in the strong coupling regime, and the quasiparticles arising from this mixing are known as cavity magnon polaritons (CMPs).<sup>8,9</sup>

PMHSs are widely investigated for advancing quantum information science. In this field, their importance lies in building quantum memories,<sup>10–16</sup> in converting microwaves to optical photons,<sup>17–21</sup> or in quantum sensing, where the detection of single magnons was

recently demonstrated.<sup>22–24</sup> CMPs recently found new applications in the field of non-Hermitian physics,<sup>25–27</sup> where they already yielded outstanding results.<sup>28</sup> Exceptional points, spots of the system's parameter space highly sensitive to external stimulations, can be probed with PMHSs,<sup>29,30</sup> and new configurations may be designed to access more exotic phenomena and study their applications.<sup>31,32</sup> The potential of hybrid systems was also shown in many other applications of quantum physics.<sup>33–37</sup>

A distinguished physical realization of this model can be obtained by hybridizing the microwave photons of a resonant cavity with the magnons of a ferrimagnetic insulator.<sup>38–42</sup> Such a scheme was implemented with multiple purposes, for example, to develop new quantum technologies with qubits,<sup>10,43</sup> or for microwave-to-optical photon conversion,<sup>20,21</sup> making it an established platform for hybrid magnonics.

In the devices described in this Letter, we employ copper cavities as a photonic resonator and Yttrium Iron Garnet (YIG) spheres as magnetic material [see Fig. 1(a)]. YIG has the exceptionally high electron spin density of  $2 \times 10^{28}$  spin/m<sup>3</sup> already at room temperature and a linewidth as narrow as 1 MHz. The latter value is matched to the one of a typical copper cavity and, thanks to the chosen spherical shape, is not affected by geometric demagnetization. Being employed in a number of microwave and rf devices, YIG is among the most

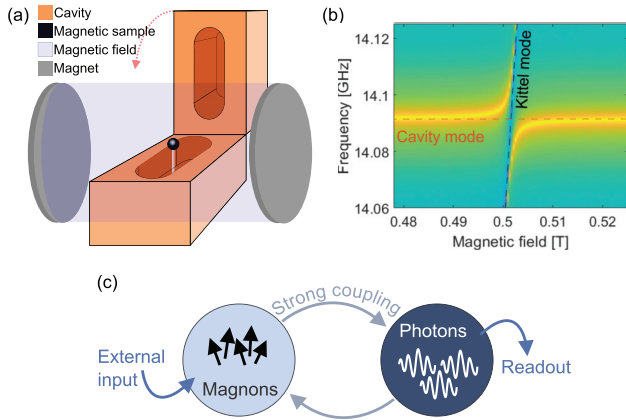


**FIG. 1.** Schematic representation of a typical PMHS (a), anticrossing curve (b), and diagram of a spin-magnetometer working principle (c). Part (a) represents a PMHS consisting of a YIG sphere housed in a microwave cavity under a static magnetic field. Plot (b) is measured with a 5 mm-diameter YIG sphere in a 14 GHz copper cavity; the color scale is in logarithmic arbitrary units, where blue to yellow is low to high transmission, and the dashed lines show the uncoupled cavity and Kittel modes.

well-known ferrites and, hence, is readily available. The magnetic sample is placed inside the cavity, where the rf magnetic field is maximum for the selected cavity mode, and is magnetized with a static field  $B_0$  perpendicular to the cavity one. In this way, the Kittel mode of magnetization couples to the microwave cavity photons, and the system exhibits the typical anticrossing dispersion relation, of which an example is shown in Fig. 1(b). The coupling strength depends on the working frequency, on the microwave mode volume, and on the number of spins involved,<sup>40</sup> but it is normally large enough to let the photon (magnon) oscillate into magnon (photon) many times before being dissipated.

This feature of the CMP to be a mixed state of microwaves and spin excitations allows one to extract information on magnons by monitoring photons. In the presence of a strong coupling, the signal transduction is efficient, i.e., without signal loss, as a spin excitation is more likely converted to a photon and detected than it is to be dissipated due to the PMHS losses [see Fig. 1(c) for a schematic diagram]. Amongst other techniques to measure spin-waves,<sup>4</sup> the use of the CMP is a particularly simple approach, which exploits the sensitivity of microwave technology and transfers it to the detection of magnons. The strong coupling makes the energy stored in a cavity dependent on the one in the material, and so an antenna coupled to the electromagnetic field of the cavity gives a simple access to the features of the spin system.<sup>44</sup> Nowadays, electronics is extremely developed, and the detection of electromagnetic radiation has been brought to the standard quantum limit of linear amplifiers. At microwave frequencies, Josephson Parametric Amplifiers (JPAs) were demonstrated to be the best devices to measure the tiniest amounts of power.<sup>45</sup> Thanks to CMPs, such precision can be shifted to a magnetic measurement, as the electromagnetic power in the cavity is highly dependent on the magnetization of the sample when the coupling strength largely exceeds the system dissipations  $g_{cm} \gg \gamma_m, \gamma_c$ . It follows that, under these conditions, the quantum-limited readout of a JPA can be exploited to detect spin excitations.

At microwave frequencies, measuring a sample’s magnetization becomes increasingly difficult because of technological limitations and fundamental problems, like, for example, radiation damping.<sup>46–48</sup> In free space, radiation damping consists of the magnetic dipole emission of a magnetized sample which, at GHz frequencies, drastically decreases the coherence time, limiting the experimental sensitivity. This effect is avoided in PMHSs, as the sample is housed in a resonant cavity, which removes the damping by inhibiting the phase space of the emission.<sup>49</sup>

For all their characteristics, PMHSs emerge as an outstanding platform for precision magnetic measurement, which are of interest for a broad range of applications as well as for approaching fundamental physics issues. Hereafter, we describe two types of spin-magnetometers, which can be designed with hybrid systems, detail their design, and report on their operation. We notice that a high occupation number of the modes permits us to treat them as classical oscillators, which is often the case throughout this work, and so we rely on a classical treatment of the fields. These devices are originally meant to measure tiniest oscillation of a sample’s magnetization, related, for example, to a Dark Matter Axion field,<sup>49,50</sup> but can be used to assess many other physical phenomena.

We now discuss the practical realisation of the devices, starting with a Transverse Spin Magnetometer (TSM). Let us now focus on a hybrid system like the one in Fig. 1, where a magnetized YIG sphere is placed in a microwave cavity. If an oscillating electromagnetic, or pseudo-electromagnetic, field  $\mathbf{b}_1$  is oriented perpendicularly to the static field, its quanta can be absorbed by the hybrid magnetic mode. As the magnetization vector  $\mathbf{M}$  precesses over the static field, an excitation lying on the precession plane can resonantly interact with it, and the system evolves according to Bloch equations,

$$\frac{d\mathbf{M}}{dt} = \gamma(\mathbf{M} \times \mathbf{b}_1)_\perp + \frac{\mathbf{M}}{T_s}, \tag{1}$$

where  $\gamma = (2\pi)28$  GHz/T is the electron gyromagnetic ratio and  $T_s$  is the system relaxation time. The driven magnetization resulting from Eq. (1) is

$$M(t) = \gamma\mu_B n_s T_s \cos(\omega_1 t), \tag{2}$$

where  $\omega_1$  is the frequency of  $\mathbf{b}_1$ . In a steady state, the power of  $\mathbf{b}_1$  is absorbed, re-emitted by the magnetization, and rapidly converted into photons thanks to the strong coupling.

The optimal experimental condition is an antenna critically coupled to the cavity, which in the steady state can extract up to half of the power deposited by the external field, resulting in

$$P_1 = \gamma\mu_B N_s \omega_1 b_1^2 T_s, \tag{3}$$

where  $N_s$  is the number of spins of the hybrid system, and the field frequency  $\omega_1$  is on resonance with one of the hybrid modes. To calculate the magnetic sensitivity of the TSM, in Eq. (3), we substitute the deposited power  $P_1$  (in Watts) with the power sensitivity of the readout electronics  $\sigma_P$  (in Watts per unit of bandwidth) and recast the equation to isolate the magnetic field. We obtain the sensitivity of the TSM,

$$\sigma_{b_1} = \sqrt{\frac{\sigma_P}{\gamma\mu_B N_s \omega_1 T_s}}, \tag{4}$$

in Tesla per unit of bandwidth, which is the field detectable in 1 s integration time with a unitary signal-to-noise ratio. Equation (4) also

shows that the spin-magnetometer sensitivity increases for larger spin-number and longer hybrid system coherence times. This suggests the use of high quality-factor cavities and samples to get a long  $T_s$  and of a large volume of high spin density magnetic material to increase  $N_s$ . In this sense, we found a good compromise in YIG. The scalability of the PMHS is of fundamental importance to obtain an increased sensitivity of the setup, as it is directly related to the increment of  $N_s$ . To this aim, we design spin-magnetometers based on the PMHS of multi-samples,<sup>51,52</sup> embedded in cylindrical cavities. To further boost the magnetic sensitivity, we reduce  $\sigma_p$  by operating the device at milli-Kelvin temperatures to reduce thermal noises and to consent the use of quantum-limited amplifiers.

Following these directions, we built a TSM whose scheme is reported in Fig. 2(a). Its PHMS comprises ten YIG spheres, all of

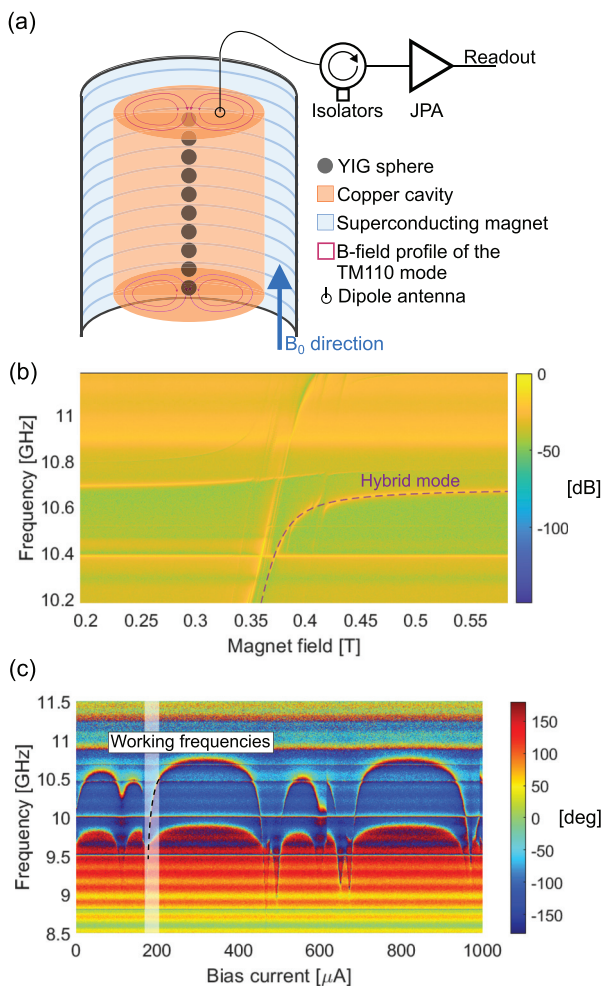


**FIG. 2.** (a) Simplified scheme of the TSM operated for an axion search<sup>52</sup> (see the text for details). (b) Anticrossing curve of the 10 YIG sphere PMHS, where the dashed line indicates the low-frequency hybrid mode monitored during the measurement. (c) Phase-current diagram of the JPC mounted in this setup; here, the dashed line shows the optimal working points of the amplifier. From plots (b) and (c), one notes that the 10.2–10.4 GHz band enables both the PMHS signal transduction and the JPA amplification.

2.1 mm-diameter, produced in-house. These are biased with a magnetic field supplied by a superconducting magnet, with 7 ppm uniformity over the volume containing the spheres. We realize the PMHS by placing the spheres along the axis of a cylindrical cavity (33 mm-diameter and 65 mm-length), allowing them to couple with the uniform rf magnetic field of the TM110 mode at 10.7 GHz.

The PMHS has been designed to reduce the effects of the magnetic dipole interaction between different spheres and of higher order magnetostatic modes. By removing the degeneracy of the TM110 mode, we limit the interference of other cavity modes; this is achieved employing a cavity with a quasi-circular section.<sup>53,54</sup> To describe this system, we used a second quantization model consisting of four coupled harmonic oscillators. We fit it to the experimental anticrossing curve of Fig. 2(b).<sup>53</sup> We then operate the magnetometer in the frequency band of 10.2–10.4 GHz, part of the lower frequency hybrid mode range, as identified by the fit (dashed line in the figure).<sup>52</sup> The operational range is matched with the working band of our Josephson Parametric Converter (JPC), i.e., a JPA formed by a Josephson ring modulator shunted with four inductances.<sup>55</sup> The JPC tuning is allowed by a small superconducting coil biased with a constant current, as shown in Fig. 2(c). The dashed lines in Fig. 2(c) include the 10.2–10.4 GHz frequency interval, showing that in this range the lower frequency hybrid mode can be monitored with our amplifier. The JPC is screened from external disturbances with different layers of superconducting and  $\mu$ -metal shields, and we verified that the solenoid providing the static field does not affect the resonance frequencies of the amplifier.

The noise temperature and gain of the electronics chain have been characterized with the injection of microwave signals of known amplitude in an antenna weakly coupled to the cavity. The effective noise temperature results in  $T_n \simeq 1$  K, which sets the noise power per unit of bandwidth  $\sigma_p = k_B T_n$ , where  $k_B$  is the Boltzmann constant. The contribution of the quantum limit to the noise budget is 0.5 K, and the remaining 0.5 K is consistent with extra noise added by the second-stage amplifier, by the losses of the wires, and by the PMHS thermodynamic temperature of  $\sim 100$  mK.<sup>52</sup> The spin number and relaxation time are obtained by fitting our model to the transmission measurements of Fig. 2(b). The measurement of  $\sigma_p$ , and of  $N_s$  and  $T_s$  through PMHS spectroscopy, allows us to calculate the sensitivity of the TSM using Eq. (4). With the parameters of this setup, we obtain a magnetic sensitivity of

$$\sigma_{b_1} = 0.9 \times 10^{-18} \left[ \left( \frac{1 \text{ K}}{T_n} \right) \left( \frac{N_s}{10^{21}} \right) \left( \frac{\omega_1/2\pi}{10.4 \text{ GHz}} \right) \left( \frac{T_s}{168 \text{ ns}} \right) \right]^{1/2} \frac{\text{T}}{\sqrt{\text{Hz}}}. \quad (5)$$

That the sensitivity given by Eq. (4) holds if the field to be detected has two characteristics: a coherence time longer than  $T_s$  and a coherence length long enough to comprise all the  $N_s$  spins.

In particular, this is the case of the field induced by Dark Matter axions,<sup>49,50</sup> which at GHz frequencies satisfies both these conditions. We used this TSM with a fixed bandwidth of 5 kHz to search for axions, obtaining a limit on their effective field of  $5.5 \times 10^{-19}$  T with about ten hours of integration.<sup>52</sup> A TSM has the advantage of being sensitive to a (pseudo)magnetic field acting on a sample, which is within the volume of a resonant cavity. In such a controlled environment, external electromagnetic disturbances are unlikely to be present,

making it an interesting testbed for fundamental physics, which are usually not subjected to such screening. However, from the point of view of the TSM possible technological employment, this feature is a limitation. In fact, the screening due to the cavity makes it difficult to expose the material to a field which is uniform and coherent over the magnetic material volume. Hence, the application of this device is probably limited to the search for new physics.

In another possible measurement scheme, a persistent oscillating  $B$ -field is parallel to the static one. We call this configuration Longitudinal Spin Magnetometer (LSM). In this configuration, the sample's magnetization precesses about a field  $B_0 + b_2 \sin(\omega_2 t)$ , where  $\omega_2$  and  $b_2$  are the oscillating field frequency and amplitude and  $t$  is the time. To illustrate the experimental arrangement, we first consider a simplified scheme including only the material and ignoring the presence of the cavity. The experimental scheme is shown in Fig. 3(a), where a sphere is surrounded by two crossed loops. Loop number 1 is used to excite the material, while loop number 2 senses the transmitted rf signal, and  $S_{21}$  plots are measured. The electron spin resonance (ESR) frequency  $\omega_m$  of the magnetized sample is modulated at the frequency  $\omega_2 \ll \omega_m$  by varying the field  $b_2 \ll B_0$ . If a monochromatic tone is applied on resonance with  $\omega_m$ , the effect of  $b_2$  is then to transfer some of the pump power, the carrier, to sidebands at frequencies  $\omega_m \pm n\omega_2$ , as schematically shown in Fig. 3(a) for  $n = 1$ . In the  $S_{21}$  spectrum of this simplified system, the amplitude of the first order sideband results in

$$\zeta_1 = \frac{\pi A_p^2 Q b_2}{2B_0}, \quad (6)$$

where  $A_p$  is the carrier amplitude and  $Q = \omega_m/\gamma_m$  the quality factor of the ESR. In a standard ESR technique, an externally applied  $b_2$  is used to detect the derivative of the ESR curve with a lock-in amplifier. Here, we invert such a scheme and search for oscillating  $b_2$ -fields by sensing the presence of sidebands. The detection of sidebands is limited by the effective noise temperature of the system determining  $\sigma_p$ , the power sensitivity already defined in the case of the TSM. The amplitude  $\zeta_1$  is given by Eq. (6) only within the linewidth of the ESR and drastically reduces for  $\omega_2 > \gamma_m$ . On the other hand, when  $\omega_2 < \gamma_m$ , extra noise induced by the pump residual amplitude modulation will increase  $\sigma_p$ . Moreover, at GHz frequencies, radiation damping broadens the linewidth of the ESR, reducing  $Q$ . As a consequence, in this configuration, the sensitivity for measuring a  $b_2$  field is poor and needs some improvements that can be engineered using PMHSs as follows.

By including a cavity, one may consider a PMHS's hybrid mode instead of a bare ESR. CMPs are immune from radiation damping; thus, we can couple the ESR to a microwave cavity to improve the detection sensitivity. We call  $\omega_p$  one of the PMHS resonant frequencies:  $\omega_p$  is also modulated by the oscillating field as  $\partial\omega_p/\partial B_0 \simeq r \times \gamma$ , where  $0 \leq r \leq 1$  is a field-dependent coefficient. When  $\omega_m$  is equal to the cavity mode resonant frequency,  $r = 1/2$ . The rf electromagnetic field of the PMHS, pumped with a tone on-resonance with one of the hybrid modes, i.e., at  $\omega_p$ , is phase-modulated through the variation of the resonant frequency and, therefore, produces sidebands too. Their amplitude drastically decreases when they depart from the resonance frequency by several linewidths, but in a PMHS, at the frequency of the second hybrid mode, one sideband does not vanish and, hence, can be detected [see Fig. 3(b)]. This device is, thus, sensitive to fields which are at frequencies  $\omega_2 \simeq 2g_{cm}$ , the splitting of the two hybrid

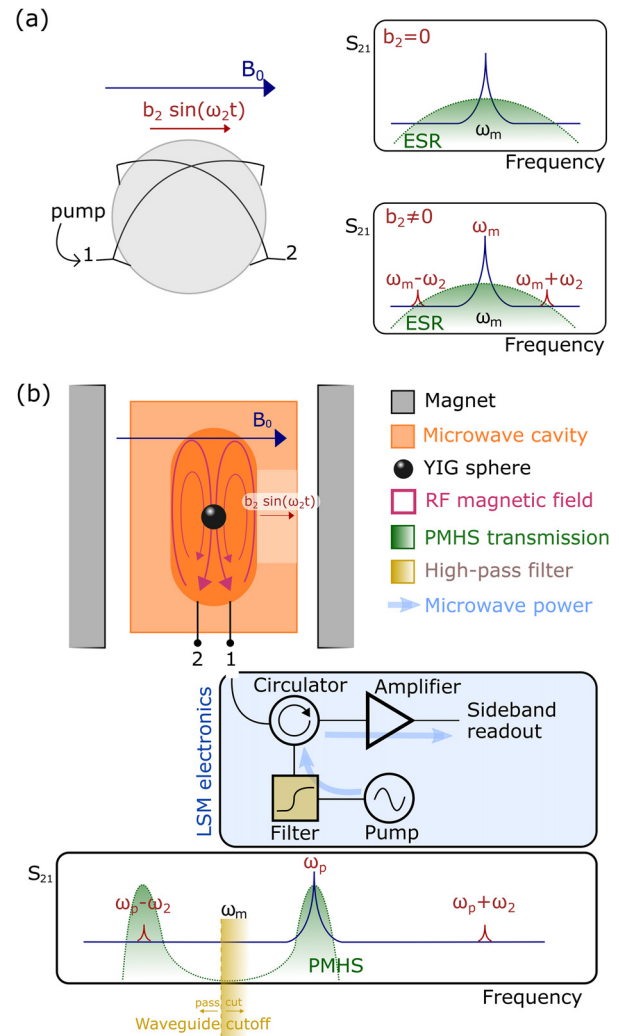


**FIG. 3.** Schematic explanation of the LSM working principles. (a) Usual design used for the detection of an ESR in a magnetic material consisting of a spherical sample (gray) surrounded by two loops in free space. The rf is fed into the system by loop antenna 1 and the output is read with the perpendicular loop 2. A pump, shown as a blue line in the spectra, is applied on-resonance with the ESR curve (green areas in the  $S_{21}$  spectra). In the absence of other fields, the result is a single peak (left plot), while with a superimposed oscillating field, the phase of the carrier is modulated by the shifting of the ESR induced by  $b_2 \sin(\omega_2 t)$ . Two sidebands, reported in the dark red in the right plot, appear at  $\omega_m \pm \omega_2$ . (b) In the LSM, a microwave tone is applied at the frequency of a hybrid mode, while the detection of a sideband, on-resonance with the second mode, probes the presence of  $b_2$ -like fields. The picture shows our room-temperature pilot setup, comprising a YIG sphere and a perforated cavity, which allows for the calibration of the spin-magnetometer. Numbers 1 and 2 are two antennas coupled to the cavity, and the side of the cavity colored in light orange represents a hole housing a loop used for calibration. See the text for further details.

modes. The possibility of detecting the sideband at a frequency much different from the pumping one allows us to drastically reduce the noise by heavily filtering the pump noise. A waveguide is a high pass filter, which can cut low frequencies by tens of dB, and that we employ

to remove the background related to the pump. If the sideband frequency  $\omega_p - \omega_2$  is below the waveguide cutoff, its amplitude is not filtered but the pump noise is [see the electronic scheme in Fig. 3(b)]. By assuming that the carrier noise can be made lower than thermal fluctuations, the latter becomes the fundamental limitation to the apparatus sensitivity. The magnetic sensitivity can be calculated by rephrasing Eq. (6) and substituting  $\zeta_1$  (the sideband power) with the readout sensitivity  $\sigma_P$  to obtain

$$\sigma_{b_2} = \frac{2B_0}{\pi r Q} \sqrt{\frac{\sigma_P}{A_p^2}}, \quad (7)$$

where, in this case,  $Q$  is the quality factor of the hybrid mode. From Eq. (7), one can see that the carrier power  $A_p^2$  can be arbitrarily increased to improve the longitudinal spin-magnetometer (LSM) magnetic sensitivity, assuming that its noise can be reduced consequently. With realistic parameters of our PMHS, one can estimate the sensitivity of a room-temperature LSM with Eq. (7), resulting in

$$\sigma_{b_2} = 10.4 \left( \frac{B_0}{0.4 \text{ T}} \right) \left( \frac{Q}{10^4} \right) \sqrt{\left( \frac{A_n^2/k_B}{300 \text{ K}} \right) \left( \frac{100 \text{ mW}}{A_p^2} \right) \frac{\text{fT}}{\sqrt{\text{Hz}}}}, \quad (8)$$

which is already competitive with state-of-the-art magnetometers like superconducting quantum interference devices (SQUIDs)<sup>56–60</sup> or spin-exchange relaxation-free (SERF) magnetometers.<sup>61–63</sup> Interestingly,  $\sigma_{b_2}$  does not depend on any extensive parameter, in contrast with  $\sigma_b$ , which relies on the total number of spins. This means that the LSM can, in principle, be miniaturized without compromising its sensitivity and removing the need for detecting a uniform field over a large volume.

A room-temperature prototype was devised to test the actual functioning of this device, and a scheme of the setup is reported in Fig. 3(b). The number of spins in the sphere, together with the shape of the rf-magnetic field of the cavity mode, set the magnetometer working frequency  $\omega_2 \simeq (2\pi) 200$  MHz. The cavity mode and the ESR resonate at 11.5 GHz (corresponding to  $B_0 = 0.4$  T), and their linewidths determine the overall quality factor of the hybrid mode  $Q = 2750$ , which is approximately the average of the two. An antenna with variable coupling is connected to the cavity to inject and extract power from the hybrid system through a circulator. A microwave pump on resonance with the high-frequency hybrid mode at  $\omega_p$  is filtered with a waveguide before being injected in the PMHS, obtaining the input power  $A_p^2 = 0.2$  mW. The signal to be detected is the PMHS output power of the sideband at  $\omega_p - \omega_2$ , the lower hybrid mode frequency. At  $\omega_p - \omega_2$ , the background is mainly thermal thanks to the filtering waveguide. The extracted signal is amplified with a low noise HEMT before being acquired with a spectrum analyzer, and the whole electronic chain has been characterized by injecting calibrated signals. The readout noise results in  $\sigma_P \simeq 4 \times 10^{-21}$  W/Hz, mostly due to room temperature thermodynamic fluctuations, and two orders of magnitude lower than the pump noise, showing that our configuration almost removes the tone-induced background. To calibrate the magnetic sensitivity of the device, we inject pico-Tesla fields at 200 MHz using a single loop on one side of the cavity, which generates a known field parallel to  $B_0$  on the YIG sphere [see Fig. 3(b)]. The setup was not optimized, but the expected losses due to imperfect matchings can be measured and accounted for by a factor  $k = 2.1$ , lowering the LSM

sensitivity. With these quantities, from Eq. (7), the expected sensitivity of the apparatus results in  $k\sigma_{b_2} = 1.9$  pT/ $\sqrt{\text{Hz}}$ . The prototype was calibrated with fields ranging from 2 to 14 pT and shows a measured sensitivity of  $2.0 \pm 0.4$  pT/ $\sqrt{\text{Hz}}$ , compatible with the estimated value.<sup>64</sup> In this setup, the loop on the side of the cavity was used for calibration, but in principle, it can be an input coil, which transduces a field to the sensitive element of the magnetometer (the magnetic sphere). This signal transduction is similar to what is usually done with SQUIDs, where an input coil is coupled to the junction loop. From Eq. (7), one notices that the LSM magnetic sensitivity benefits from high quality factors, low readout noise, and high pump power. The former feature is related to the quality factors of the PMHS, which should comprise narrow-linewidth cavities and magnetic materials to improve the magnetometer sensitivity. The latter two essentially depend on the microwave electronics of the setup. Since the sensitivity is size-independent, miniaturization can be foreseen by using 2D printed resonators and small quantities of material. Eventually, we mention that multiplexing was also shown to be a viable option in similar devices.<sup>65–67</sup>

The sensitivity of the two PMHS-based magnetometers is limited by the noise of the readout noise temperature, which ultimately consists of quantum fluctuations.<sup>68</sup> We foresee the use of a broadband Travelling Wave JPA<sup>69–71</sup> to overcome the standard JPA limitation of being resonant. To overcome the quantum-limit, one may rely on single photon or magnon counters, which are unaffected by this issue, rather than on linear amplifiers.

A downside of both the magnetometers is that their resonant nature implies a reduced bandwidth, limited to the linewidth of a hybrid mode. Nevertheless, as the resonant frequencies of the hybrid modes can be changed with a tuning of the  $B_0$  field, the band of both the TSM and LSM can be extended. In particular, for TSMs, this changes the hybrid mode frequency [see Fig. 2(b)] and, for LSMs, is a variation of the vacuum-Rabi splitting  $2g_{cm}$ . Since the working band of the two magnetometers is controlled by the dynamics of CMPs, the latter was studied in a separate work.<sup>72</sup>

In conclusion, we described and operated two different types of CMP-based magnetometers, which show an outstanding magnetic sensitivity. The TSM is a device that benefits from its scalability, which lowers the minimum detectable magnetization oscillations. We believe that it is more suitable for studying fundamental physics, for instance, in the search for Axions, where Dark Matter can be described as a wide, uniform, and persistent rf field acting on the electron spins. The LSM is a device of simpler application, as it can precisely detect faint magnetic fields localized on a small spin ensemble. Its sensitivity relies on the design and engineering of the PMHS, which can be further developed to reach remarkable sensitivity improvements. We mention that its usage to search for Axions is immediate and that a single LSM can scan a broad Axion-mass range by changing the CMP vacuum-Rabi splitting. We showed that the unique features of PMHSs make them suitable to assess fundamental physics problems, and we envision more future applications of these systems as testbeds for precision magnetometry.

The authors would like to acknowledge the contribution of the QUAX collaboration in the development of these devices. We also thank Enrico Berto, Andrea Benato, Fulvio Calao, and Mario Tessaro for their help in the building of the experimental setups

and, in particular, for the aid with the mechanics, cryogenics, and electronics of the apparatuses. We acknowledge the support of INFN-Laboratori Nazionali di Legnaro for hosting all the experimental setups described in this work and for the availability of large quantities of liquid helium.

## DATA AVAILABILITY

The data supporting the findings of this work are available from the corresponding author upon reasonable request.

## REFERENCES

- <sup>1</sup>A. A. Clerk, K. W. Lehnert, P. Bertet, J. R. Petta, and Y. Nakamura, "Hybrid quantum systems with circuit quantum electrodynamics," *Nat. Phys.* **16**, 257–267 (2020).
- <sup>2</sup>D. Lachance-Quirion, Y. Tabuchi, A. Gloppe, K. Usami, and Y. Nakamura, "Hybrid quantum systems based on magnonics," *Appl. Phys. Express* **12**, 070101 (2019).
- <sup>3</sup>S. Haroche and J.-M. Raimond, *Exploring the Quantum: Atoms, Cavities, and Photons* (Oxford University Press, 2006).
- <sup>4</sup>A. V. Chumak, V. I. Vasyuchka, A. A. Serga, and B. Hillebrands, "Magnon spintronics," *Nat. Phys.* **11**, 453–461 (2015).
- <sup>5</sup>C. L. Degen, F. Reinhard, and P. Cappellaro, "Quantum sensing," *Rev. Mod. Phys.* **89**, 035002 (2017).
- <sup>6</sup>G. Kurizki, P. Bertet, Y. Kubo, K. Mølmer, D. Petrosyan, P. Rabl, and J. Schmiedmayer, "Quantum technologies with hybrid systems," *Proc. Natl. Acad. Sci. U. S. A.* **112**, 3866–3873 (2015).
- <sup>7</sup>Y. R. Shen and N. Bloembergen, "Interaction between light waves and spin waves," *Phys. Rev.* **143**, 372–384 (1966).
- <sup>8</sup>C. Kittel, *Introduction to Solid State Physics*, 8th ed. (Wiley, 2004).
- <sup>9</sup>D. F. Walls and G. J. Milburn, *Quantum Optics* (Springer Science & Business Media, 2007).
- <sup>10</sup>Y. Tabuchi, S. Ishino, A. Noguchi, T. Ishikawa, R. Yamazaki, K. Usami, and Y. Nakamura, "Quantum magnonics: The magnon meets the superconducting qubit," *C. R. Phys.* **17**, 729–739 (2016).
- <sup>11</sup>X. Zhang, C.-L. Zou, N. Zhu, F. Marquardt, L. Jiang, and H. X. Tang, "Magnon dark modes and gradient memory," *Nat. Commun.* **6**, 8914 (2015).
- <sup>12</sup>D. I. Schuster, A. P. Sears, E. Ginossar, L. DiCarlo, L. Frunzio, J. J. L. Morton, H. Wu, G. A. D. Briggs, B. B. Buckley, D. D. Awschalom, and R. J. Schoelkopf, "High-cooperativity coupling of electron-spin ensembles to superconducting cavities," *Phys. Rev. Lett.* **105**, 140501 (2010).
- <sup>13</sup>A. Ghirri, C. Bonizzoni, D. Gerace, S. Sanna, A. Cassinese, and M. Affronte, "YBCO microwave resonators for strong collective coupling with spin ensembles," *Appl. Phys. Lett.* **106**, 184101 (2015).
- <sup>14</sup>O. O. Soykal and M. E. Flatté, "Strong field interactions between a nanomagnet and a photonic cavity," *Phys. Rev. Lett.* **104**, 077202 (2010).
- <sup>15</sup>A. Ghirri, C. Bonizzoni, F. Troiani, N. Buccheri, L. Beverina, A. Cassinese, and M. Affronte, "Coherently coupling distinct spin ensembles through a high- $T_c$  superconducting resonator," *Phys. Rev. A* **93**, 063855 (2016).
- <sup>16</sup>K. Heshami, D. G. England, P. C. Humphreys, P. J. Bustard, V. M. Acosta, J. Nunn, and B. J. Sussman, "Quantum memories: Emerging applications and recent advances," *J. Mod. Opt.* **63**, 2005–2028 (2016).
- <sup>17</sup>H. J. Kimble, "The quantum internet," *Nature* **453**, 1023–1030 (2008).
- <sup>18</sup>L. A. Williamson, Y.-H. Chen, and J. J. Longdell, "Magneto-optic modulator with unit quantum efficiency," *Phys. Rev. Lett.* **113**, 203601 (2014).
- <sup>19</sup>X. Fernandez-Gonzalvo, Y.-H. Chen, C. Yin, S. Rogge, and J. J. Longdell, "Coherent frequency up-conversion of microwaves to the optical telecommunications band in an Er: YSO crystal," *Phys. Rev. A* **92**, 062313 (2015).
- <sup>20</sup>R. Hisatomi, A. Osada, Y. Tabuchi, T. Ishikawa, A. Noguchi, R. Yamazaki, K. Usami, and Y. Nakamura, "Bidirectional conversion between microwave and light via ferromagnetic magnons," *Phys. Rev. B* **93**, 174427 (2016).
- <sup>21</sup>C. Braggio, G. Carugno, M. Guarise, A. Ortolan, and G. Ruoso, "Optical manipulation of a magnon-photon hybrid system," *Phys. Rev. Lett.* **118**, 107205 (2017).
- <sup>22</sup>D. Lachance-Quirion, Y. Tabuchi, S. Ishino, A. Noguchi, T. Ishikawa, R. Yamazaki, and Y. Nakamura, "Resolving quanta of collective spin excitations in a millimeter-sized ferromagnet," *Sci. Adv.* **3**, e1603150 (2017).
- <sup>23</sup>D. Lachance-Quirion, S. P. Wolski, Y. Tabuchi, S. Kono, K. Usami, and Y. Nakamura, "Entanglement-based single-shot detection of a single magnon with a superconducting qubit," *Science* **367**, 425–428 (2020).
- <sup>24</sup>S. P. Wolski, D. Lachance-Quirion, Y. Tabuchi, S. Kono, A. Noguchi, K. Usami, and Y. Nakamura, "Dissipation-based quantum sensing of magnons with a superconducting qubit," [arXiv:2005.09250](https://arxiv.org/abs/2005.09250) (2020).
- <sup>25</sup>C. M. Bender, "Making sense of non-Hermitian Hamiltonians," *Rep. Prog. Phys.* **70**, 947–1018 (2007).
- <sup>26</sup>C. M. Bender and S. Boettcher, "Real spectra in non-Hermitian Hamiltonians having  $\mathcal{PT}$  symmetry," *Phys. Rev. Lett.* **80**, 5243–5246 (1998).
- <sup>27</sup>C. E. Rüter, K. G. Makris, R. El-Ganainy, D. N. Christodoulides, M. Segev, and D. Kip, "Observation of parity-time symmetry in optics," *Nat. Phys.* **6**, 192–195 (2010).
- <sup>28</sup>D. Zhang, X.-Q. Luo, Y.-P. Wang, T.-F. Li, and J. Q. You, "Observation of the exceptional point in cavity magnon-polaritons," *Nat. Commun.* **8**, 1368 (2017).
- <sup>29</sup>X. Zhang, K. Ding, X. Zhou, J. Xu, and D. Jin, "Experimental observation of an exceptional surface in synthetic dimensions with magnon polaritons," *Phys. Rev. Lett.* **123**, 237202 (2019).
- <sup>30</sup>K. Ding, G. Ma, M. Xiao, Z. Q. Zhang, and C. T. Chan, "Emergence, coalescence, and topological properties of multiple exceptional points and their experimental realization," *Phys. Rev. X* **6**, 021007 (2016).
- <sup>31</sup>G.-Q. Zhang and J. Q. You, "Higher-order exceptional point in a cavity magnonics system," *Phys. Rev. B* **99**, 054404 (2019).
- <sup>32</sup>Y. Cao and P. Yan, "Exceptional magnetic sensitivity of  $\mathcal{PT}$ -symmetric cavity magnon polaritons," *Phys. Rev. B* **99**, 214415 (2019).
- <sup>33</sup>J. W. Rao, S. Kaur, B. M. Yao, E. R. J. Edwards, Y. T. Zhao, X. Fan, D. Xue, T. J. Silva, Y. S. Gui, and C.-M. Hu, "Analogue of dynamic hall effect in cavity magnon polariton system and coherently controlled logic device," *Nat. Commun.* **10**, 2934 (2019).
- <sup>34</sup>N. J. Lambert, J. A. Haigh, S. Langenfeld, A. C. Doherty, and A. J. Ferguson, "Cavity-mediated coherent coupling of magnetic moments," *Phys. Rev. A* **93**, 021803 (2016).
- <sup>35</sup>Y.-P. Wang, J. W. Rao, Y. Yang, P.-C. Xu, Y. S. Gui, B. M. Yao, J. Q. You, and C.-M. Hu, "Nonreciprocity and unidirectional invisibility in cavity magnonics," *Phys. Rev. Lett.* **123**, 127202 (2019).
- <sup>36</sup>Y.-P. Wang, G.-Q. Zhang, D. Zhang, T.-F. Li, C.-M. Hu, and J. Q. You, "Bistability of cavity magnon polaritons," *Phys. Rev. Lett.* **120**, 057202 (2018).
- <sup>37</sup>H. Y. Yuan, P. Yan, S. Zheng, Q. Y. He, K. Xia, and M.-H. Yung, "Steady bell state generation via magnon-photon coupling," *Phys. Rev. Lett.* **124**, 053602 (2020).
- <sup>38</sup>H. Huebl, C. W. Zollitsch, J. Lotze, F. Hocke, M. Greifenstein, A. Marx, R. Gross, and S. T. B. Goennenwein, "High cooperativity in coupled microwave resonator ferrimagnetic insulator hybrids," *Phys. Rev. Lett.* **111**, 127003 (2013).
- <sup>39</sup>Y. Tabuchi, S. Ishino, T. Ishikawa, R. Yamazaki, K. Usami, and Y. Nakamura, "Hybridizing ferromagnetic magnons and microwave photons in the quantum limit," *Phys. Rev. Lett.* **113**, 083603 (2014).
- <sup>40</sup>X. Zhang, C.-L. Zou, L. Jiang, and H. X. Tang, "Strongly coupled magnons and cavity microwave photons," *Phys. Rev. Lett.* **113**, 156401 (2014).
- <sup>41</sup>M. Goryachev, W. G. Farr, D. L. Creedon, Y. Fan, M. Kostylev, and M. E. Tobar, "High-cooperativity cavity QED with magnons at microwave frequencies," *Phys. Rev. Appl.* **2**, 054002 (2014).
- <sup>42</sup>D. Zhang, X.-M. Wang, T.-F. Li, X.-Q. Luo, W. Wu, F. Nori, and J. Q. You, "Cavity quantum electrodynamics with ferromagnetic magnons in a small yttrium-iron-garnet sphere," *npj Quantum Inf.* **1**, 15014 (2015).
- <sup>43</sup>Y. Tabuchi, S. Ishino, A. Noguchi, T. Ishikawa, R. Yamazaki, K. Usami, and Y. Nakamura, "Coherent coupling between a ferromagnetic magnon and a superconducting qubit," *Science* **349**, 405–408 (2015).
- <sup>44</sup>T. Wolz, A. Stehli, A. Schneider, I. Boverter, R. Macêdo, A. V. Ustinov, M. Kläui, and M. Weides, "Introducing coherent time control to cavity magnon-polariton modes," *Commun. Phys.* **3**, 3 (2020).
- <sup>45</sup>A. Roy and M. Devoret, "Introduction to parametric amplification of quantum signals with Josephson circuits," *C. R. Phys.* **17**, 740–755 (2016).
- <sup>46</sup>S. Bloom, "Effects of radiation damping on spin dynamics," *J. Appl. Phys.* **28**, 800–805 (1957).
- <sup>47</sup>M. Augustine, "Transient properties of radiation damping," *Prog. Nucl. Magn. Reson. Spectrosc.* **40**, 111–150 (2002).

- <sup>48</sup>N. Bloembergen and R. V. Pound, "Radiation damping in magnetic resonance experiments," *Phys. Rev.* **95**, 8–12 (1954).
- <sup>49</sup>R. Barbieri, C. Braggio, G. Carugno, C. Gallo, A. Lombardi, A. Ortolan, R. Pengo, G. Ruoso, and C. Speake, "Searching for galactic axions through magnetized media: The quax proposal," *Phys. Dark Universe* **15**, 135–141 (2017).
- <sup>50</sup>R. Barbieri, M. Cerdonio, G. Fiorentini, and S. Vitale, "Axion to magnon conversion. A scheme for the detection of galactic axions," *Phys. Lett. B* **226**, 357–360 (1989).
- <sup>51</sup>N. Crescini, D. Alesini, C. Braggio, G. D. Carugno, D. Gioacchino, C. S. Gallo, U. Gambardella, C. Gatti, G. Iannone, G. Lamanna, C. Ligi, A. Lombardi, A. Ortolan, S. Pagano, R. Pengo, G. Ruoso, C. C. Speake, and L. Taffarello, "Operation of a ferromagnetic axion haloscope at  $m_a = 58 \mu\text{eV}$ ," *Eur. Phys. J. C* **78**, 703 (2018).
- <sup>52</sup>N. Crescini, D. Alesini, C. Braggio, G. Carugno, D. D'Agostino, D. Di Gioacchino, P. Falferi, U. Gambardella, C. Gatti, G. Iannone, C. Ligi, A. Lombardi, A. Ortolan, R. Pengo, G. Ruoso, and L. Taffarello, "Axion search with a quantum-limited ferromagnetic haloscope," *Phys. Rev. Lett.* **124**, 171801 (2020).
- <sup>53</sup>N. Crescini, C. Braggio, G. Carugno, A. Ortolan, and G. Ruoso, "Coherent coupling between multiple ferrimagnetic spheres and a microwave cavity in the quantum-limit," [arXiv:2007.08908](https://arxiv.org/abs/2007.08908) (2020).
- <sup>54</sup>R. Macêdo, R. C. Holland, P. G. Baity, K. L. Livesey, R. L. Stamps, M. P. Weides, and D. A. Bozhko, "An electromagnetic approach to cavity spintronics," [arXiv:2007.11483](https://arxiv.org/abs/2007.11483) (2020).
- <sup>55</sup>N. Roch, E. Flurin, F. Nguyen, P. Morfin, P. Campagne-Ibarcq, M. H. Devoret, and B. Huard, "Widely tunable, nondegenerate three-wave mixing microwave device operating near the quantum limit," *Phys. Rev. Lett.* **108**, 147701 (2012).
- <sup>56</sup>R. C. Jaklevic, J. Lambe, A. H. Silver, and J. E. Mercereau, "Quantum interference effects in Josephson tunneling," *Phys. Rev. Lett.* **12**, 159–160 (1964).
- <sup>57</sup>S. N. Erné, H. Hahlbohm, and H. Lübbig, "Theory of rf-biased superconducting quantum interference device for nonhysteretic regime," *J. Appl. Phys.* **47**, 5440–5442 (1976).
- <sup>58</sup>M. Aprili, "The nanosquid makes its debut," *Nat. Nanotechnol.* **1**, 15–16 (2006).
- <sup>59</sup>R. Kleiner, D. Koelle, F. Ludwig, and J. Clarke, "Superconducting quantum interference devices: State of the art and applications," *Proc. IEEE* **92**, 1534–1548 (2004).
- <sup>60</sup>C. John and B. I. Alex, *The SQUID Handbook* (John Wiley & Sons, Ltd, 2005).
- <sup>61</sup>I. K. Kominis, T. W. Kornack, J. C. Allred, and M. V. Romalis, "A subfemtotesla multichannel atomic magnetometer," *Nature* **422**, 596–599 (2003).
- <sup>62</sup>I. M. Savukov, S. J. Seltzer, M. V. Romalis, and K. L. Sauer, "Tunable atomic magnetometer for detection of radio-frequency magnetic fields," *Phys. Rev. Lett.* **95**, 063004 (2005).
- <sup>63</sup>D. Budker and M. Romalis, "Optical magnetometry," *Nat. Phys.* **3**, 227–234 (2007).
- <sup>64</sup>N. Crescini, G. Ruoso, and G. Carugno, "Phase-modulated cavity magnon polaritons as a precise magnetic field probe" (unpublished).
- <sup>65</sup>S. Kempf, M. Wegner, A. Fleischmann, L. Gastaldo, F. Herrmann, M. Papst, D. Richter, and C. Enss, "Demonstration of a scalable frequency-domain readout of metallic magnetic calorimeters by means of a microwave squid multiplexer," *AIP Adv.* **7**, 015007 (2017).
- <sup>66</sup>K. D. Irwin and K. W. Lehnert, "Microwave squid multiplexer," *Appl. Phys. Lett.* **85**, 2107–2109 (2004).
- <sup>67</sup>J. A. B. Mates, G. C. Hilton, K. D. Irwin, L. R. Vale, and K. W. Lehnert, "Demonstration of a multiplexer of dissipationless superconducting quantum interference devices," *Appl. Phys. Lett.* **92**, 023514 (2008).
- <sup>68</sup>S. K. Lamoreaux, K. A. van Bibber, K. W. Lehnert, and G. Carosi, "Analysis of single-photon and linear amplifier detectors for microwave cavity dark matter axion searches," *Phys. Rev. D* **88**, 035020 (2013).
- <sup>69</sup>A. L. Cullen, "A travelling-wave parametric amplifier," *Nature* **181**, 332–332 (1958).
- <sup>70</sup>C. Macklin, K. O'Brien, D. Hover, M. E. Schwartz, V. Bolkhovskoy, X. Zhang, W. D. Oliver, and I. Siddiqi, "A near-quantum-limited Josephson traveling-wave parametric amplifier," *Science* **350**, 307–310 (2015).
- <sup>71</sup>L. Planat, A. Ranadive, R. Dassonneville, J. Puertas Martínez, S. Léger, C. Naud, O. Buisson, W. Hasch-Guichard, D. M. Basko, and N. Roch, "Photonic-crystal Josephson traveling-wave parametric amplifier," *Phys. Rev. X* **10**, 021021 (2020).
- <sup>72</sup>N. Crescini, C. Braggio, G. Carugno, R. D. Vora, A. Ortolan, and G. Ruoso, "Magnon-driven dynamics of a hybrid system excited with ultrafast optical pulses," *Commun. Phys.* **3**, 164 (2020).